ACS APPLIED MATERIALS & INTERFACES

Research Article

www.acsami.org

Flexible Infrared Responsive Multi-Walled Carbon Nanotube/Form-Stable Phase Change Material Nanocomposites

Yunming Wang,[†,§] Hongyi Mi,[‡,§] Qifeng Zheng,[†] Zhenqiang Ma,[*,‡] and Shaoqin Gong[*,†]

[†]Department of Biomedical Engineering, Wisconsin Institute for Discovery, and Materials Science Program and [‡]Department of Electrical and Computer Engineering, University of Wisconsin−Madison, Madison, Wisconsin 53706, United States

Supporting Information

ABSTRACT: Flexible infrared (IR)-responsive materials, such as polymer nanocomposites, that exhibit high levels of IR responses and short response times are highly desirable for various IR sensing applications. However, the IR-induced photoresponses of carbon nanotube (CNT)/polymer nanocomposites are typically limited to 25%. Herein, we report on a family of unique nanocomposite films consisting of multi-walled carbon nanotubes (MWCNTs) uniformly distributed in a form-stable phase change material (PCM) that exhibited rapid, dramatic, reversible, and cyclic IR-regulated responses in air. The 3 wt % MWCNT/PCM nanocomposite films demonstrated cyclic, IR-regulated on/off electrical conductivity ratios of 11.6 ± 0.6 and 570.0 ± 70.5 times at IR powers of 7.3 and 23.6 mW/mm^2, respectively. The excellent performances exhibited by the MWCNT/PCM nanocomposite films were largely attributed to the IR-regulated cyclic and reversible form-stable phase transitions occurring in the PCM matrix due to MWCNT's excellent photoabsorption and thermal conversion capabilities, which subsequently affected the thickness of the interfacial PCM between adjacent conductive MWCNTs and thus the electron tunneling efficiency between the MWCNTs. Our findings suggest that these unique MWCNT/PCM nanocomposites offer promising new options for high-performance and flexible optoelectronic devices, including thermal imaging, IR sensing, and optical communication.

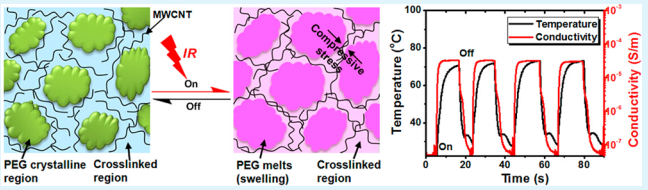

KEYWORDS: *IR responsive electrical conductivity, polymer nanocomposites, multi-walled carbon nanotubes, form-stable phase change materials, flexible photoelectronics*

INTRODUCTION

Carbon nanomaterials, including carbon nanotubes (CNTs) and graphenes, have generated a great deal of interest in the fields of electronics and photonics due to their unique properties.[1−7] To achieve an efficient photoresponse, the radiation absorber should have a high absorptivity and low heat capacity.[8,9] CNTs are very sensitive to radiation due to their low density, high surface area, and negligible heat capacity.[10,11] In particular, CNTs possess unique infrared (IR) responsive properties, including strong photoabsorption, photothermal conversion, and photoacoustic generation due to their π-conjugated structures, thereby making them a promising candidate for IR detecting applications.[12−17] IR sensing provides attractive applications in the field of optoelectronics, such as thermography, night vision, medical imaging, and surveillance.[7,16,18,19] There have been previous studies on IR photoresponsive CNTs[6] and CNT/polymer nanocomposites,[14,20,21] in which the IR-induced response in electrical conductivity was mainly attributed to the photoexcitation of CNTs producing extra charge carriers[22] and/or the thermal effect causing a change of CNT conductivity.[23−26] However, these materials often exhibit relatively low IR sensitivities and may require complex fabrication processes that tend to hinder their potential applications.

Herein, we report a simple and versatile method of fabricating nanocomposite thin films consisting of multi-walled carbon nanotubes (MWCNTs) uniformly distributed in a form-stable phase change material (PCM). In comparison with previously reported IR sensing materials based on CNT/polymer composites,[14,20,21] which typically produce an IR response of less than 25%, the newly developed MWCNT/PCM nanocomposites exhibited much more dramatic as well as cyclic IR photoresponses. In particular, the 3 wt % MWCNT/PCM nanocomposite films demonstrated cyclic, IR-regulated on/off electrical conductivity ratios of 11.6 ± 0.6 and 570.0 ± 70.5 times at IR powers of 7.3 and 23.6 mW/mm^2, respectively. The dramatic IR photoresponses observed with the MWCNT/PCM nanocomposite films were largely attributed to the reversible phase transition processes governed by the IR irradiation. These reversible melting and recrystallization transitions occurring with the crystalline polyethylene glycol (PEG) regions embedded in the form-stable PCM matrix subsequently affected the thickness of the interfacial PCM between adjacent conductive MWCNTs and thus the electron tunneling efficiency between the MWCNTs, thereby triggering a dramatic change in the electrical conductivity. The superior sensing performances exhibited by the MWCNT/PCM nanocomposite films, coupled with their form-stable and bendable

Received: August 1, 2015
Accepted: September 15, 2015
Published: September 15, 2015

DOI: 10.1021/acsami.5b07064
ACS Appl. Mater. Interfaces 2015, 7, 21602−21609

Scheme 1. Synthesis and Fabrication Process for the Surface-Functionalized MWCNT (Step 1), PCM (Step 2), and MWCNT/PCM Nanocomposites (Step 3)

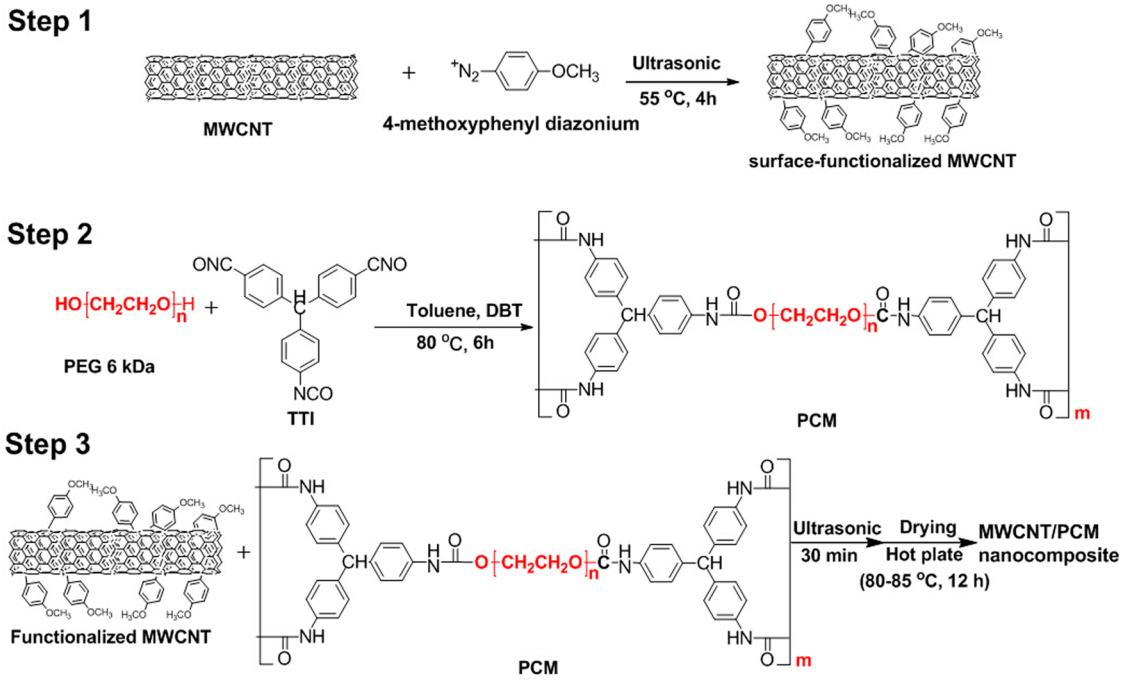

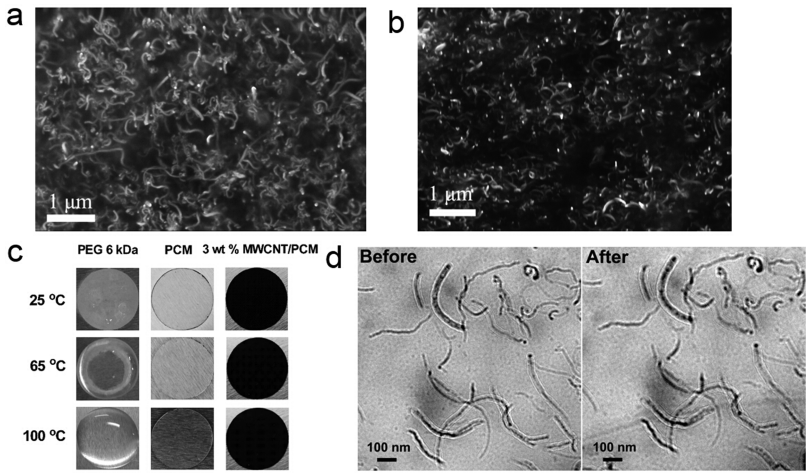

Figure 1. (a) The SEM image (top view) of the 3 wt % MWCNT/PCM nanocomposite film. (b) The SEM image (cross-section view) of the 3 wt % MWCNT/PCM nanocomposite film. (c) Comparison of the macroscopic morphology of the films formed by pure PEG, PCM, and 3 wt % MWCNT/PCM nanocomposites at different temperatures. The PCM and MWCNT/PCM nanocomposite films exhibited form-stable phase transition behaviors. (d) The TEM images of the 3 wt % MWCNT/PCM nanocomposites taken at room temperature before and after IR irradiation (23.6 mW/mm^2 for 10 s).

characteristics, suggest that such IR responsive nanomaterials can offer numerous applications, including flexible IR sensing, thermal imaging, and optical communication. This work can lead to a new generation of flexible optical and thermal electronics based on carbon nanofiller/polymer nanocomposites.

RESULTS AND DISCUSSION

CNTs with high aspect ratios tend to form bundles and entanglements due to their strong intertube van der Waals interactions.[27] Therefore, it is challenging to produce uniform CNT dispersions in organic solvents and polymer matrices,[22] which hinders their applications.[28,29] Scheme 1 shows a schematic representation of the fabrication process for the MWCNT/PCM nanocomposite films. To obtain MWCNT/PCM nanocomposite films with evenly distributed MWCNTs, MWCNTs were functionalized with *p*-methoxyphenyl diazonium salts (see Scheme 1). The *p*-methoxyphenyl functionalized MWCNTs had excellent dispersibility in DMF, which was one of the two solvents used to prepare the MWCNT/PCM nanocomposite films. The form-stable PCM was synthesized with difunctional polyethylene glycol (PEG, 6 kDa) and trifunctional triphenylmethanetriisocyanate (TTI) (see Scheme 1). Panels a and b Figure 1 are the top and cross-section views, respectively, of the MWCNT/PCM nanocomposite film under SEM, which indicate that the MWCNTs

DOI: 10.1021/acsami.5b07064
ACS Appl. Mater. Interfaces 2015, 7, 21602−21609

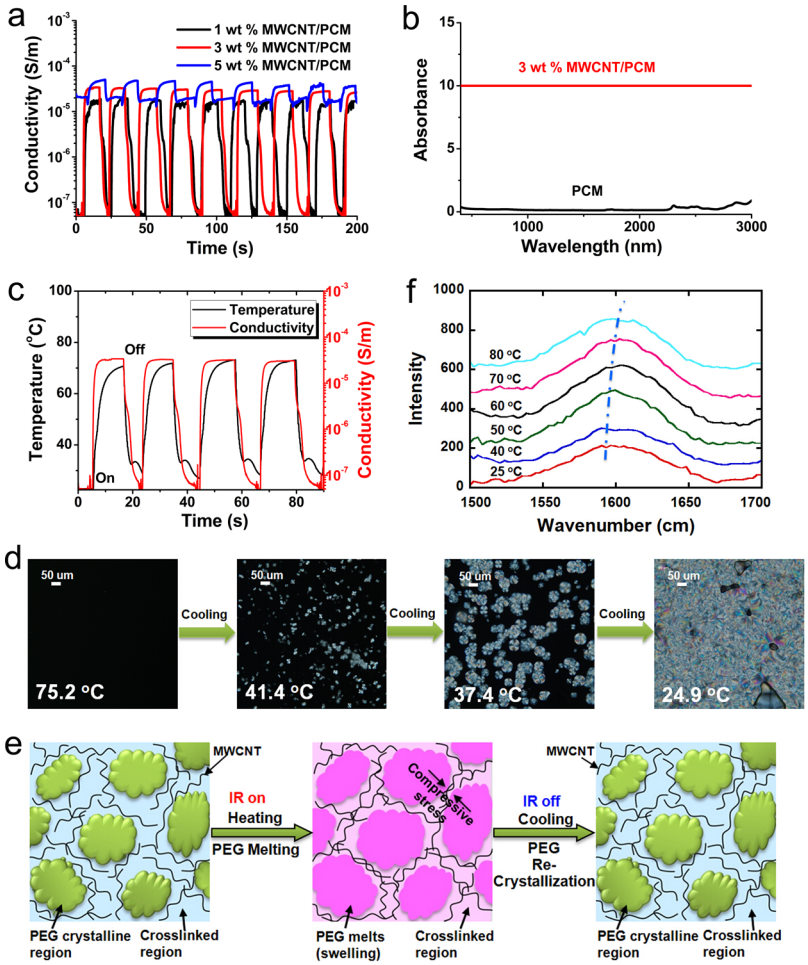

Figure 2. (a) The cyclic electrical conductivity responses of the three types of MWCNT/PCM nanocomposite films with 1, 3, and 5 wt % MWCNTs, respectively, to IR illumination (23.6 mW/mm^2, sample size: 0.5 × 0.5 × 0.15 mm^3). (b) IR absorbance spectra of the PCM (black) and 3 wt % MWCNT/PCM nanocomposite film (red). (c) The cyclic electrical conductivity and temperature responses of the 3 wt % MWCNT/PCM nanocomposite film to IR (23.6 mW/mm^2, sample size: 0.5 × 0.5 × 0.15 mm^3). (d) Polarized microscope images of the PCM during the cooling process. The degree of PEG crystallinity in PCM alone was 58.4%. (e) Conceptual illustration of the cyclic, dramatic, and reversible electrical conductivity changes observed in the MWCNT/PCM nanocomposite films regulated by IR. The degrees of PEG crystallinity in the MWCNT/PCM nanocomposites ranged from 51 to 53%. Upon IR illumination, the localized and microscopic PEG crystalline regions melted, causing a localized volume expansion (~14.5%), and subsequently creating a compressive stress on the cross-linked elastic regions where the MWCNTs resided, which led to a reduction in the thickness of the interfacial PCM between adjacent conductive MWCNTs, thereby enhancing the electron tunneling efficiency and ultimately the electrical conductivity of the MWCNT/PCM nanocomposite films. This form-stable and reversible phase transition process (i.e., the localized PEG melting and recrystallization process) occurring in the PCM induces cyclic and reversible IR-regulated electrical conductivity changes. (f) The Raman spectra of the 3 wt % MWCNT/PCM nanocomposite taken at different temperatures.

were evenly distributed in the PCM matrix. This is essential to obtain reproducible and consistent material properties, including electrical conductivity. The uniform dispersion of the MWCNTs in the PCM matrix was mainly attributed to the strong van der Waals forces present among PCM, toluene, and the *p*-methoxyphenyl groups of the surface-functionalized MWCNTs. Figure 1c shows the macroscopic morphology of the films formed by pure PEG (6 kDa), PCM, and 3 wt % MWCNT/PCM nanocomposites at different temperatures. Unlike the pure PEG film that exhibits a clear solid-to-liquid phase transition when the temperature was increased from room temperature to 65.0 °C and then to 100.0 °C, both the PCM film and the MWCNT/PCM nanocomposite film exhibited form-stable phase transitions; namely, these films retained a solid form at the macroscopic level during the microscopic and localized PEG crystallite melting process because the PEG molecules formed cross-links with the trifunctional TTI, the other component within the PCM structure. In addition, the PCM film became transparent at higher temperatures due to the melting of the microscopic and localized PEG crystallites. Figure 1d shows the TEM images for the same location of the MWCNT/PCM nanocomposite before and after IR illumination (23.6 mW/mm^2 for 10 s) at room temperature. These TEM images taken at room temperatures did not show any apparent changes in the distribution of the MWCNTs in the MWCNT/PCM nanocomposite before and after IR illumination. This suggests that the change in the microstructure of the nanocomposite induced by IR irradiation was recovered upon removal of the IR light, which is consistent with the reversible electrical conductivity regulation observed during the multiple cycles of IR irradiation discussed later.

The nanocomposite films demonstrated a dramatic, reversible, cyclic, and rapid IR photoresponse in electrical

DOI: 10.1021/acsami.5b07064
ACS Appl. Mater. Interfaces 2015, 7, 21602−21609

conductivity. Figure 2a shows the real time cyclic IR photoresponse of the MWCNT/PCM nanocomposite films with different MWCNT loading contents (i.e., 1, 3, and 5 wt % in air, power density: 23.6 mW/mm^2, sample size: 0.5 × 0.5 × 0.15 mm^3). Although all three types of nanocomposite films demonstrated a similar trend in IR responses—namely, the electrical conductivity increased upon IR illumination and then decreased after IR removal—the magnitude of the changes in the electrical conductivity varied significantly with the loading content of MWCNT. More specifically, the on/off (in terms of IR illumination) electrical conductivity ratios were 418.0, 570.0, and 2.4, corresponding to 1, 3, and 5 wt % MWCNT content in the nanocomposites, respectively. The initial electrical conductivity of the MWCNT/PCM nanocomposite films measured at room temperature before IR illumination is shown in Figure S1. The 3 wt % nanocomposite films had an initial electrical conductivity only slightly higher than that of the 1 wt % nanocomposite films. However, the initial electrical conductivity of the nanocomposite films with 5 wt % MWCNT was 2 orders of magnitude higher than that of the nanocomposite films with 1 and 3 wt % MWCNT, suggesting that the 5 wt % nanocomposite had already reached the electrical percolation threshold.[30] Namely, the 5 wt % nanocomposite film already had a good electrical conductive path before IR illumination. The electrical conductivity of the conductive nanofiller/polymer nanocomposites is more sensitive to the structural change of the conductive nanofiller network induced by various factors, such as internal stress, when the conductive nanofiller loading content is close to the electrical percolation threshold. This could explain why the on/off (in terms of IR illumination) electrical conductivity ratios of the nanocomposite films initially increased (from 418.0 to 570.0 for 1 and 3 wt % MWCNTs) and then decreased (from 570.0 to 2.4 for 3 and 5 wt % MWCNTs) with the MWCNT loading content. Another observation with the cyclic IR response under repeated on/off IR illumination shown in Figure 2a was that the profile features of all cycles measured were virtually identical. These cyclic performances reflected the excellent reversibility and reliability of the MWCNT/PCM nanocomposite films.

It is well-known that CNTs can absorb IR light efficiently and consequently convert photoenergy to thermal energy, thereby causing an increase in the temperature of the CNT/polymer nanocomposites.[13,17] Indeed, as shown in Figure 2b, the MWCNT/PCM nanocomposite films had excellent IR absorbance. Figure 2c shows the combined real-time cyclic temperature and electrical conductivity changes of the nanocomposite films modulated via on/off IR illumination (23.6 mW/mm^2). The temperature response matched with the electrical conductivity response reasonably well. Under IR illumination, the temperature of the nanocomposite rapidly increased from room temperature (~23.0 °C) to ~72.0 °C in ~12 s. Furthermore, although the temperature of the 3 wt % MWCNT/PCM nanocomposite film exceeded the melting temperature of PEG crystallites in the nanocomposite (i.e., 62.6 °C) as measured by DSC (Figure S2 or Table S1), the film remained solid at a macroscopic level during the entire heating process despite the localized melting of the PEG crystallites.

After IR was turned off, the temperature of the nanocomposite films immediately dropped from its peak temperature. It is also interesting to note that near the end of the cooling process (upon IR removal), there was a small temperature bump around 33.7 °C. This was caused by the exothermic PEG recrystallization process that occurred during the cooling process.[13,31] Additional information on the phase transition behavior of the nanocomposites analyzed using differential scanning calorimetry (DSC) is shown in Table S1 and Figure S2. Figure S3 shows the X-ray diffraction (XRD) patterns of the PEG and 3 wt % MWCNT/PCM nanocomposite confirming the presence of PEG crystallites in the nanocomposite film. As presented in Table S1, the degrees of PEG crystallinity in the MWCNT/PCM nanocomposites ranged from 51 to 53%.

The IR-induced electrical conductivity increase (up to 25%) observed in several CNT/polymer composites was attributed to the photoexcitation of charge carriers in CNTs and/or the thermal effect on the conductivity of CNTs.[14,20,21] For this study, the dramatic, reversible, and cyclic IR photoresponses (up to 57,000%) observed in the MWCNT/PCM nanocomposite films were largely attributed to the effect of the reversible localized PEG melting and recrystallization phase transition processes regulated by IR illumination on the thickness of the interfacial PCM between adjacent conductive MWCNTs and thus the electron tunneling efficiency between the MWCNTs in the PCM matrix. For the phase change effect on the IR photoresponse to be further demonstrated, the formation of the PEG crystallites in the pure PCM during the cooling process was observed using a polarized microscope as shown in Figure 2d. During the cooling process, spherulite-like PEG crystallites were formed with sizes that were dependent on the cooling rate.[32] As shown in Table S1, the recrystallization temperatures (T_c) of the MWCNT/PCM nanocomposites during cooling were lower than that of the pure PCM, and the degrees of PEG crystallinity of the nanocomposites (both χ_m and χ_c) were also lower than that of the PCM. These findings are consistent with previous reports that nanoparticles, including MWCNT and montmorillonite, do not act like nucleating agents in the PEG matrix.[33] Therefore, MWCNTs were largely distributed within the cross-linked (as shown in Scheme 1, TTI is trifunctional) noncrystalline regions surrounding the localized PEG crystalline regions. This observation is further supported by the TEM images taken at room temperatures (Figure 1d), suggesting no apparent change in the distribution of the MWCNTs before and after the cyclic IR irradiation. If the MWCNTs were present in the PEG crystalline regions that underwent the melting process during the cyclic IR irradiation process, the distribution of the MWCNTs taken at room temperature would likely be changed after the cycle. In contrast, if the MWCNTs were distributed in the cross-linked elastic regions that do not undergo the melting process during the cyclic IR irradiation process, which is essential for the form-stable PCM (see Figure 1c), it is not surprising then to find that the MWCNT distribution before and after the cyclic IR irradiation taken at room temperature did not change.

Figure 2e is a schematic representation of the potential effect of cyclic PEG melting and recrystallization (i.e., localized and microscopic PEG crystallites melting upon IR irradiation or recrystallizing within the MWCNT/PCM nanocomposite upon IR removal) on the distribution of the conductive MWCNT network within the PCM matrix. During the heating process (i.e., upon IR illumination), the microscopic and localized PEG crystalline regions within the PCM matrix melted, thereby leading to a localized volume expansion and subsequently generating a compressive internal stress on the cross-linked elastic regions where the MWCNTs resided. The densities of

DOI: 10.1021/acsami.5b07064
ACS Appl. Mater. Interfaces 2015, 7, 21602−21609

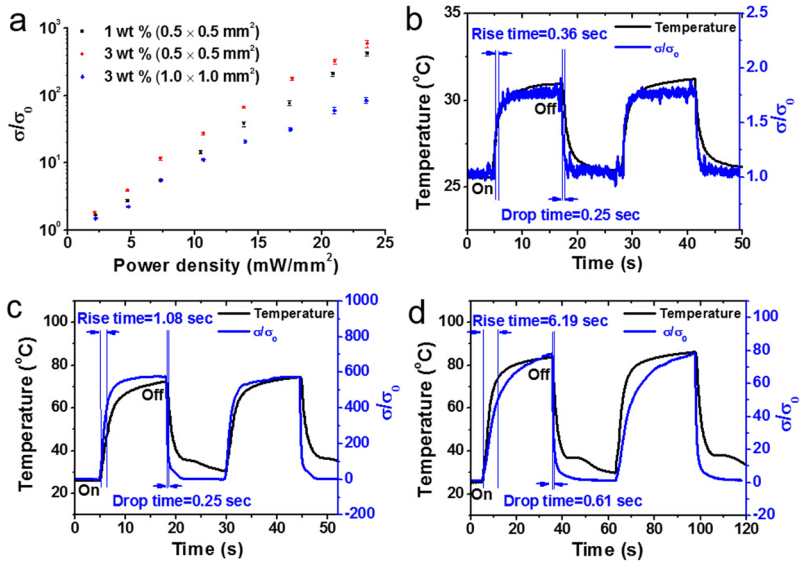

Figure 3. (a) The IR power density dependence of the on/off electrical conductivity ratios (σ/σ_0) for nanocomposite films with different MWCNT loading contents (i.e., 1 vs 3 wt %) or different sample sizes (i.e., 0.5 × 0.5 mm^2 vs 1.0 × 1.0 mm^2, see Figure S4). The photoresponses of the on/off electrical conductivity ratios (σ/σ_0) and temperature profiles of the 3 wt % MWCNT/PCM nanocomposite at the following conditions: (b) IR power density: 2.2 mW/mm^2, size: 0.5 × 0.5 mm^2; (c) IR power density: 23.6 mW/mm^2, size: 0.5 × 0.5 mm^2; and (d) IR power density: 23.6 mW/mm^2, size: 1.0 × 1.0 mm^2. Note: The rise time represents the time it takes for the response to reach 63.2% of its final value during the heating process. The drop time represents the time it takes for the response to reach 36.8% of its initial value during the cooling process.

the crystalline PEG regions at room temperature and the PEG melts (~68.0 °C) are approximately 1.243 and 1.086 g/mL, respectively; thus, the localized volume expansion induced by the localized and microscopic PEG melting was approximately 14.5%.[34] Because of the presence of this compressive internal stress, the thickness of the interfacial PCM between adjacent conductive MWCNTs was reduced, leading to an enhanced electron tunneling efficiency between the MWCNTs[35] and subsequently a drastic increase in the electrical conductivity of the MWCNT/PCM nanocomposite film. During the cooling process (i.e., upon removal of the IR light), the molten PEG regions recrystallized, thereby eliminating the compressive internal stress experienced by the cross-linked elastic regions that was generated during the IR heating process, which subsequently increased the thickness of the interfacial PCM between adjacent conductive MWCNTs, thereby leading to a reduction in the electron tunneling efficiency between the MWCNTs, and hence a decrease in the electrical conductivity.

This proposed mechanism for the IR-induced cyclic and dramatic electrical conductivity regulation observed in the MWCNT/PCM nanocomposites was further supported by the Raman analyses. The G band of MWCNTs, a measure of its phonon vibration mode, is sensitive to stress applied to the MWCNTs. In response to the stress, the G band position of MWCNTs shown in the Raman spectrum is shifted.[36,37] Figure 2f shows the spectra of the MWCNT/PCM nanocomposites taken at different temperatures. As shown in Figure 2f, the G band peaks of the MWCNTs in the Raman spectra at 1590.0 cm^{-1} upshifted ~10.6 cm^{-1} when the temperature increased from room temperature to 70.0 °C, suggesting that the MWCNTs in the MWCNT/PCM nanocomposites were subjected to compressive stress during the heating process.[36,37] According to a previous systematic study, the pressure/stress coefficient of the MWCNTs' G band peak was 4.25 cm^{-1}/GPa.[38] Consequently, the magnitude of the compressive internal stress generated during the PEG melting process that was exerted on the MWCNTs embedded in the cross-linked elastic regions was calculated to be 2.49 GPa at 70.0 °C. In other words, the Raman analyses confirmed the presence of a compressive internal stress generated during the IR heating process due to volume expansion resulting from melting of the PEG crystalline regions. Furthermore, the similar trends exhibited by the IR responses of the temperature and electrical conductivity, as shown in Figure 2c, further supports this proposed mechanism. Lastly, it is worth noting that such a dramatic cyclic IR response in electrical conductivity induced by cyclic phase transitions regulated by IR illumination was achieved while the MWCNT/PCM nanocomposite film retained its overall solid form during the entire heating and cooling process. Such form-stable IR responsive materials offer additional advantages that may lead to simplified manufacturing processes and less contingent requirements for device packaging.

Figure 3a presents the dependence of the electrical conductivity regulation on the incident IR power density for the nanocomposite films with different MWCNT loading contents (i.e., 1 and 3 wt %) or different sample sizes (i.e., 0.5 × 0.5 mm^2 or 1.0 × 1.0 mm^2). Overall, the photoresponses of the electrical conductivity ratios for the 1 wt % nanocomposites were smaller than that of the 3 wt % nanocomposites, suggesting that the 3 wt % nanocomposites had a better final conductive network under IR illumination than the 1 wt % nanocomposites as discussed previously. The on/off electrical conductivity ratios increased with the IR power density in a nearly logarithmic linear fashion for both types of nanocomposites (i.e., 1 and 3 wt % MWCNTs with a sample size of 0.5 × 0.5 mm^2). For instance, for the 3 wt % nanocomposite, the on/off electrical conductivity ratios corresponding to the IR power density of 2.2, 7.3, and 23.6 mW/mm^2 were 1.8, 11.6, and 570.0 times, respectively. Panels b and c in Figure 3 show the photoresponses of the on/off electrical conductivity ratios and the corresponding temperature profiles of the 3 wt %

DOI: 10.1021/acsami.5b07064
ACS Appl. Mater. Interfaces 2015, 7, 21602−21609

nanocomposites with a sample size of 0.5 × 0.5 mm^2 at an IR power density of 2.2 and 23.6 mW/mm^2, respectively. At an IR power density of 2.2 mW/mm^2, the maximum temperature of the nanocomposite film was only 31.2 °C, which was well below the peak melting temperature of the PEG crystallites (Table S1 and Figure S2a). In contrast, at an IR power density (23.6 mW/mm^2), the maximum temperature of the nanocomposite film reached ∼72.0 °C, suggesting that the degree of the PEG phase change should be much higher at a higher incident IR power density compared with the lower incident IR power density. This comparison validates the concept that the dramatic on/off electrical conductivity ratios observed for the 3 wt % nanocomposite films at 23.6 mW/mm^2 (i.e., 570.0 times) was largely due to the cyclic melting and recrystallization phase transition behavior.

As shown in Figure 3a, the dimensions of the 3 wt % MWCNT/PCM nanocomposite films used for the measurement also had a major influence on the on/off electrical conductivity ratios. At the same IR power density, the on/off electrical conductivity ratios of the nanocomposite films with a size of 0.5 × 0.5 mm^2 was consistently much higher than those of the films with a size of 1.0 × 1.0 mm^2. For instance, at an IR power density of 23.6 mW/mm^2, the magnitude of change in the electrical conductivity for the nanocomposite films with a size of 0.5 × 0.5 mm^2 and 1.0 × 1.0 mm^2 was 570.0 and 74.0 times, respectively, at the same IR illumination time (∼12 s). With a much longer IR illumination time (∼30 s), the magnitude of change in the electrical conductivity for the nanocomposite film with a size of 1.0 × 1.0 mm^2 sample reached 84 times, which was still much smaller than that of the 0.5 × 0.5 mm^2 nanocomposite film. This was likely due to the fact that, at the same IR power density, the PEG melting and recrystallization phase transition process may have been activated more easily in the nanocomposite film with the smaller dimensions per mass. As shown in Figure 3d, the final temperature of the 1.0 × 1.0 mm^2 sample (∼82.0 °C) was slightly higher than that of the 0.5 × 0.5 mm^2 sample (∼72.0 °C). This was attributed to the fact that the smaller sample had a higher surface-to-volume ratio allowing for more efficient thermal exchange between the sample itself and the surrounding environment. Figure S5 shows the DSC measurements for samples with different dimensions/masses (i.e., 5.02 mg and 20.77 mg) at different heating/cooling rates (i.e., 5 and 20 °C/min). At the same heating and cooling rate, the peak PEG melting temperature was higher, whereas the peak PEG recrystallization temperature for the larger sample was lower than with the smaller sample. Furthermore, this temperature difference increased at a higher heating/cooling rate. Table S2 lists the percentage of the phase transition at two temperatures, namely 72.0 and 82.0 °C, calculated based on the ratio of the phase transition enthalpy (i.e., $\Delta H_T/\Delta H_{total}$; see Figure S5). It is clear that both the sample size and the heating and cooling rates could have a significant impact on the phase transition behaviors of the nanocomposite films likely due to thermal conduction issues. This finding may help explain why the nanocomposite film with a size of 0.5 × 0.5 mm^2 exhibited a much larger IR response than that with a size of 1.0 × 1.0 mm^2 considering the fact that the heating rates for these experiments were extremely high (i.e., ∼250 °C/min).

To explore the IR photoresponse sensitivity, we studied the rise time (with IR on) and drop time (with IR off) of the MWCNT/PCM nanocomposites to obtain a 63.2% change in the magnitude of the electrical conductivity regulated by on/off IR illumination, which is shown in Figure 3b–d. As the IR power density increased, the rise time of the 0.5 × 0.5 mm^2 nanocomposite film increased from ∼0.36 s (under 2.2 mW/mm^2 with a total conductivity change of 1.8 times) to ∼1.08 s (under 23.6 mW/mm^2 with a total conductivity change of 570.0 times). When the sample size increased from 0.5 × 0.5 mm^2 to 1.0 × 1.0 mm^2, the rise time also increased from 1.08 to 6.19 s. Hence, nanocomposite films with smaller dimensions were more sensitive and responded faster to IR illumination than those with larger dimensions.

Additionally, according to thermogravimetric analysis (TGA), the MWCNT/PCM nanocomposites exhibited good thermal stability (Figure S6). The temperature of the most significant weight loss for the 3 wt % MWCNT/PCM nanocomposite occurred between 376.0 and 427.0 °C. The MWCNT/PCM nanocomposite films also exhibited robust flexibility and could easily be stretched and bent (Figure S7). The tensile testing results for the 3 wt % MWCNT/PCM nanocomposites are shown in Figure S7b and Table S3. These data demonstrate that the 3 wt % MWCNT/PCM nanocomposite films have excellent mechanical properties, thereby making them desirable for flexible optical–electrical applications.

CONCLUSIONS

IR responsive MWCNT/PCM nanocomposite films exhibiting reversible, cyclic, dramatic, and rapid electrical conductivity changes were fabricated and fully characterized. The reversible, cyclic, and dramatic changes observed with IR-regulated on/off electrical conductivity ratios (up to 570.0 times) were largely attributed to the reversible IR-regulated localized PEG melting and recrystallization processes experienced by the form-stable PCM matrix due to MWCNT's excellent photoabsorption and thermal conversion capabilities, which subsequently affected the thickness of the interfacial PCM between adjacent conductive MWCNTs and thus the electron tunneling efficiency between the MWCNTs. It was also found that the magnitude of the changes in the electrical conductivity ratios as well as the response time (or sensitivity) of these nanocomposite films regulated by IR irradiation depended on a number of factors including the MWCNT loading content in the nanocomposite films, the IR power density, and the sample size of the nanocomposite films measured. Finally, the MWCNT/PCM nanocomposite films also possessed desirable mechanical and thermal properties, thereby making these unique nanocomposites a promising material family for high-performance flexible optoelectronic applications, including IR sensing, thermal imaging, and optical communication.

METHODS AND MATERIALS

Materials. Multiwalled carbon nanotubes (MWCNTs) (inner diameter: 4 nm, length: >1 μm, number of walls: 3–15, bulk density: 140–230 kg/m^3, purity: >99%) were purchased from Bayer Materials Science AG (51368 Leverkusen, Germany). Triphenylmethanetriisocyanate (TTI, Boc Sciences, NY, USA) and dibutyltin dilaurate (DBT, Alfa Aesar, MA, USA) were used as received. *p*-Anisidine, sodium dodecyl sulfonate, and toluene were purchased from Fisher Scientific (Bellefonte, PA). Polyethylene glycol (PEG 6 kDa) and *N*,*N*-dimethylformamide (DMF) were of analytical grade and purchased from Sigma-Aldrich (St. Louis, MO). PEG (6 kDa) was dried at 80.0 °C under a high vacuum (0.012 MPa) for 48 h before use. Toluene was dried for 48 h using a 5 Å molecular sieve and then distilled prior to use. All other reagents were of analytical grade.

DOI: 10.1021/acsami.5b07064
ACS Appl. Mater. Interfaces 2015, 7, 21602–21609

Synthesis of Surface-Functionalized MWCNTs. MWCNTs were functionalized with 4-methoxyphenyl diazonium according to a method described in the literature.[39] Scheme 1 (Step 1) shows the synthesis process used to surface-functionalize the MWCNTs. First, 4-methoxyphenyl diazonium was synthesized by dissolving 5 mmol *p*-anisidine in 15 mL of DI water, followed by adding 1.25 mL of concentrated hydrochloric acid and 5 mmol sodium nitrite under constant stirring for 30 min. Then, 100 mg of MWCNTs and 10 mg of sodium dodecyl sulfonate (used as a surfactant) were dispersed in 100 mL of deionized water. Thereafter, the freshly made 4-methoxyphenyl diazonium solution was added to the MWCNT solution dropwise under sonication. The mixture was ultrasonicated at 300 W for 4 h at 55.0 °C and then stirred overnight at ambient temperature. It was then filtered and washed successively with water and ethanol. The resulting product (i.e., the functionalized MWCNTs) were dried overnight in a freeze dryer.

Synthesis of the Form-Stable Phase Change Material (PCM). Scheme 1 (Step 2) shows the synthesis route of the PCM. The synthesis reaction was conducted in flame-dried glassware under an inert nitrogen (N_2) atmosphere. Then, 3.0 g of dried PEG (6 kDa), 122.5 mg of TTI, and 1.5 mg of dibutyltin dilaurate (DBT) were mixed in freshly distilled toluene and stirred for 6 h in a N_2 atmosphere at 80.0−85.0 °C to obtain form-stable PCM.

Synthesis of the MWCNT/PCM Nanocomposites. A specific amount of functionalized MWCNTs was dispersed in DMF via ultrasonication (Hielscher UP 400S, Bernau bei Berlin, Germany, 300 W, 30 min). The resulting MWCNT solution and the PCM toluene solution described earlier were mixed thoroughly using a Hielscher UP 400S probe ultrasonic sonicator (see Scheme 1). The mixture was ultrasonicated at 300 W for 30 min at 60.0 °C to obtain a well-dispersed suspension. Subsequently, the functionalized MWCNT/PCM solution was heated on a hot plate at 80.0−85.0 °C. To control the rate of solvent evaporation, and thus facilitate the formation of the MWCNT/PCM nanocomposite films with uniformly distributed MWCNTs, we covered the top of the Petri dish containing the MWCNT/PCM solution with grade 2 filter paper (thickness: 0.26 mm, pore diameter: 8 μm). The resulting MWCNT/PCM nanocomposite film was further dried for 24 h at 80.0 °C under vacuum (0.0010 mbar).

Characterization. The chemical structures of the MWCNTs, PCM, and MWCNT/PCM nanocomposites were analyzed using a Fourier transform infrared (FTIR) spectrophotometer (Bruker Tensor 27 FT-IR) at room temperature. The electrical conductivities of the nanocomposite films with a thickness of 0.15 mm and varying surface areas (e.g., 0.5 × 0.5 mm^2 or 1.0 × 1.0 mm^2) were measured using an HP4155 semiconductor analyzer (voltage bias: 5 V). The nanocomposite film was set on a Teflon plate, and its two ends were covered with silver paste serving as electrical contacts. The light source was an LED with an emission peak of 813 nm. The film temperature was measured using a K-type thermocouple. A silver wire detector was placed beneath the film to measure the temperature accurately. Scanning electron microscopy (LEO GEMINI 1530 SEM, Zeiss, Germany) and transmission emission microscopy (TEM, FEI Tecnai T30) were used to characterize the microstructure of the graphene/PCM nanocomposites. For TEM analysis, the sample (~70 nm in thickness) was prepared using a microtome (Reichert UltraCut E, NY USA). Differential scanning calorimetry (DSC) analyses were performed in a N_2 atmosphere using a Q20 DSC thermal analyzer (TA Instruments, DE, USA) from 0 to 100.0 °C at a N_2 flow rate of 20 mL/min. To study the effects of temperature on the structure and morphology of the PEG, PCM, and MWCNT/PCM nanocomposite films, we took digital images of these films periodically while they were heated on a hot stage from 25.0 to 100.0 °C (5 °C/min). The thermal stability of these films were characterized via thermogravimetric analysis (TGA) using a TGA/Q50 thermal analyzer (TA Instruments, DE, USA). Approximately 10 mg of the nanocomposite films were heated from 30.0 to 700.0 °C at a heating rate of 10 °C/min in a N_2 atmosphere. X-ray diffraction (XRD, Bruker D8-Discovery) analyses were carried out on the samples from 5° to 80° (diffraction angles, 2θ). UV−vis absorbance was measured using a Varian Cary 5000 Bio UV−visible spectrophotometer. Polarized optical images of the crystalline PCM were taken using a polarized light microscope (EN60950, Diagnostic Instruments Inc., MI, USA). The Raman spectra of the MWCNT/PCM nanocomposite were measured using a LabRAM Aramis microspectrometer.

■ ASSOCIATED CONTENT

Supporting Information

The Supporting Information is available free of charge on the ACS Publications website at DOI: 10.1021/acsami.5b07064.

Additional experimental details and characterization data, including initial electrical conductivity, DSC, XRD, TGA, FTIR, and NMR analyses as well as mechanical properties (PDF)

■ AUTHOR INFORMATION

Corresponding Authors

*E-mail: mazq@engr.wisc.edu. Tel: +1-608-261-1095.
*E-mail: sgong@engr.wisc.edu. Tel: +1-608-316-4311.

Author Contributions

§Y.W. and H.M. contributed equally to this work.

Notes

The authors declare no competing financial interest.

■ ACKNOWLEDGMENTS

This research was supported in part by AFOSR PECASE Grant #FA9550-09-1-0482. The AFOSR program manager is Dr. Gernot Pomrenke. The authors thank Mr. Guojun Chen for his help with the TEM analysis.

■ REFERENCES

(1) De Volder, M. F. L.; Tawfick, S. H.; Baughman, R. H.; Hart, A. J. Carbon Nanotubes: Present and Future Commercial Applications. *Science* **2013**, *339*, 535−539.

(2) Nanotechnology: Nanotubes Form a Complex Circuit, *Nature* **2014**; Vol. *509*, pp 536−53710.1038/509536d.

(3) Shulaker, M. M.; Hills, G.; Patil, N.; Wei, H.; Chen, H.-Y.; Wong, H. S. P.; Mitra, S. Carbon Nanotube Computer. *Nature* **2013**, *501*, 526−530.

(4) Klimov, N. N.; Jung, S.; Zhu, S.; Li, T.; Wright, C. A.; Solares, S. D.; Newell, D. B.; Zhitenev, N. B.; Stroscio, J. A. Electromechanical Properties of Graphene Drumheads. *Science* **2012**, *336*, 1557−1561.

(5) Herring, P. K.; Hsu, A. L.; Gabor, N. M.; Shin, Y. C.; Kong, J.; Palacios, T.; Jarillo-Herrero, P. Photoresponse of an Electrically Tunable Ambipolar Graphene Infrared Thermocouple. *Nano Lett.* **2014**, *14*, 901−907.

(6) John, J.; Muthee, M.; Yogeesh, M.; Yngvesson, S. K.; Carter, K. R. Suspended Multiwall Carbon Nanotube-Based Infrared Sensors via Roll-to-Roll Fabrication. *Adv. Opt. Mater.* **2014**, *2*, 581−587.

(7) Wang, Z. L.; Wu, W. Nanotechnology-Enabled Energy Harvesting for Self-Powered Micro-/Nanosystems. *Angew. Chem., Int. Ed.* **2012**, *51*, 11700−11721.

(8) Richards, P. L. Bolometers for Infrared and Millimeter Waves. *J. Appl. Phys.* **1994**, *76*, 1−24.

(9) Xiao, L.; Zhang, Y. Y.; Wang, Y.; Liu, K.; Wang, Z.; Li, T. Y.; Jiang, Z.; Shi, J. P.; Liu, L. A.; Li, Q. Q.; Zhao, Y. G.; Feng, Z. H.; Fan, S. S.; Jiang, K. L. A Polarized Infrared Thermal Detector Made From Super-Aligned Multiwalled Carbon Nanotube Films. *Nanotechnology* **2011**, *22*, 025502.

(10) Aliev, A. E.; Guthy, C.; Zhang, M.; Fang, S.; Zakhidov, A. A.; Fischer, J. E.; Baughman, R. H. Thermal Transport in MWCNT Sheets and Yarns. *Carbon* **2007**, *45*, 2880−2888.

(11) Hepplestone, S. P.; Ciavarella, A. M.; Janke, C.; Srivastava, G. P. Size and Temperature Dependence of the Specific Heat Capacity of Carbon Nanotubes. *Surf. Sci.* **2006**, *600*, 3633−3636.

DOI: 10.1021/acsami.5b07064
ACS Appl. Mater. Interfaces 2015, 7, 21602−21609

(12) Kohlmeyer, R. R.; Chen, J. Wavelength-Selective, IR Light-Driven Hinges Based on Liquid Crystalline Elastomer Composites. *Angew. Chem., Int. Ed.* **2013**, *52*, 9234−9237.
(13) Wang, Y.; Tang, B.; Zhang, S. Single-Walled Carbon Nanotube/Phase Change Material Composites: Sunlight-Driven, Reversible, Form-Stable Phase Transitions for Solar Thermal Energy Storage. *Adv. Funct. Mater.* **2013**, *23*, 4354−4360.
(14) Pradhan, B.; Setyowati, K.; Liu, H. Y.; Waldeck, D. H.; Chen, J. Carbon Nanotube - Polymer Nanocomposite Infrared Sensor. *Nano Lett.* **2008**, *8*, 1142−1146.
(15) Vijayakumar, C.; Balan, B.; Kim, M.-J.; Takeuchi, M. Noncovalent Functionalization of SWNTs with Azobenzene-Containing Polymers: Solubility, Stability, and Enhancement of Photoresponsive Properties. *J. Phys. Chem. C* **2011**, *115*, 4533−4539.
(16) Zhang, J.; Strano, M. S. Single-Walled Carbon Nanotube Near-Infrared Fluorescent Sensors for Biological Systems. In *Nanoplatform-Based Molecular Imaging*; John Wiley & Sons, Inc., 2011; pp 217−232.
(17) Chen, L.; Zou, R.; Xia, W.; Liu, Z.; Shang, Y.; Zhu, J.; Wang, Y.; Lin, J.; Xia, D.; Cao, A. Electro- and Photodriven Phase Change Composites Based on Wax-Infiltrated Carbon Nanotube Sponges. *ACS Nano* **2012**, *6*, 10884−10892.
(18) Chen, J. Actuators and Infrared Sensors Based on Carbon Nanotube-Polymer Composites. In *Carbon Nanotube-Polymer Composites*; The Royal Society of Chemistry, 2013; Chapter 2, pp 22−50.
(19) Oueiny, C.; Berlioz, S.; Perrin, F.-X. Carbon Nanotube−Polyaniline Composites. *Prog. Polym. Sci.* **2014**, *39*, 707−748.
(20) Pradhan, B.; Kohlmeyer, R. R.; Setyowati, K.; Owen, H. A.; Chen, J. Advanced Carbon Nanotube/Polymer Composite Infrared Sensors. *Carbon* **2009**, *47*, 1686−1692.
(21) Liu, X.-Q.; Li, Y.-L.; Lin, Y.-W.; Yang, S.; Guo, X.-F.; Li, Y.; Yang, J.; Chen, E.-Q. Composites of Functional Poly(phenylacetylene)s and Single-Walled Carbon Nanotubes: Preparation, Dispersion, and Near Infrared Photoresponsive Properties. *Macromolecules* **2013**, *46*, 8479−8487.
(22) Fujigaya, T.; Morimoto, T.; Niidome, Y.; Nakashima, N. NIR Laser-Driven Reversible Volume Phase Transition of Single-Walled Carbon Nanotube/Poly(N-isopropylacrylamide) Composite Gels. *Adv. Mater.* **2008**, *20*, 3610−3614.
(23) Behabtu, N.; Young, C. C.; Tsentalovich, D. E.; Kleinerman, O.; Wang, X.; Ma, A. W. K.; Bengio, E. A.; ter Waarbeek, R. F.; de Jong, J. J.; Hoogerwerf, R. E.; Fairchild, S. B.; Ferguson, J. B.; Maruyama, B.; Kono, J.; Talmon, Y.; Cohen, Y.; Otto, M. J.; Pasquali, M. Strong, Light, Multifunctional Fibers of Carbon Nanotubes with Ultrahigh Conductivity. *Science* **2013**, *339*, 182−186.
(24) Chen, J.; Gui, X.; Wang, Z.; Li, Z.; Xiang, R.; Wang, K.; Wu, D.; Xia, X.; Zhou, Y.; Wang, Q.; Tang, Z.; Chen, L. Superlow Thermal Conductivity 3D Carbon Nanotube Network for Thermoelectric Applications. *ACS Appl. Mater. Interfaces* **2011**, *4*, 81−86.
(25) Itkis, M. E.; Borondics, F.; Yu, A.; Haddon, R. C. Bolometric Infrared Photoresponse of Suspended Single-Walled Carbon Nanotube Films. *Science* **2006**, *312*, 413−416.
(26) Rivadulla, F.; Mateo-Mateo, C.; Correa-Duarte, M. A. Layer-by-Layer Polymer Coating of Carbon Nanotubes: Tuning of Electrical Conductivity in Random Networks. *J. Am. Chem. Soc.* **2010**, *132*, 3751−3755.
(27) Thess, A.; Lee, R.; Nikolaev, P.; Dai, H. J.; Petit, P.; Robert, J.; Xu, C. H.; Lee, Y. H.; Kim, S. G.; Rinzler, A. G.; Colbert, D. T.; Scuseria, G. E.; Tomanek, D.; Fischer, J. E.; Smalley, R. E. Crystalline Ropes of Metallic Carbon Nanotubes. *Science* **1996**, *273*, 483−487.
(28) Kim, O.-K.; Je, J.; Baldwin, J. W.; Kooi, S.; Pehrsson, P. E.; Buckley, L. J. Solubilization of Single-Wall Carbon Nanotubes by Supramolecular Encapsulation of Helical Amylose. *J. Am. Chem. Soc.* **2003**, *125*, 4426−4427.
(29) Miyako, E.; Nagata, H.; Hirano, K.; Hirotsu, T. Carbon Nanotube−Polymer Composite for Light-Driven Microthermal Control. *Angew. Chem., Int. Ed.* **2008**, *47*, 3610−3613.
(30) Mohiuddin, M.; Hoa, S. V. Temperature Dependent Electrical Conductivity of CNT−PEEK Composites. *Compos. Sci. Technol.* **2011**, *72*, 21−27.
(31) Sari, A. Thermal Energy Storage Properties of Mannitol-Fatty Acid Esters as Novel Organic Solid-Liquid Phase Change Materials. *Energy Convers. Manage.* **2012**, *64*, 68−78.
(32) He, C. L.; Sun, J. R.; Zhao, T.; Hong, Z. K.; Zhuang, X. L.; Chen, X. S.; Jing, X. B. Formation of a Unique Crystal Morphology for the Poly(Ethylene Glycol)-Poly(Epsilon-Caprolactone) Diblock Copolymer. *Biomacromolecules* **2006**, *7*, 252−258.
(33) Strawhecker, K. E.; Manias, E. Crystallization Behavior of Poly(ethylene Oxide) in the Presence of Na Plus Montmorillonite Fillers. *Chem. Mater.* **2003**, *15*, 844−849.
(34) Seo, A.; Schaefer, T. Melt Agglomeration with Polyethylene Glycol Beads at a low Impeller Speed in a High Shear Mixer. *Eur. J. Pharm. Biopharm.* **2001**, *52*, 315−325.
(35) Liu, L. Y.; Yang, Y. G.; Zhang, Y. F. A Study on the Electrical Conductivity of Multi-Walled Carbon Nanotube Aqueous Solution. *Phys. E (Amsterdam, Neth.)* **2004**, *24*, 343−348.
(36) Kumar, R.; Cronin, S. B. Raman Scattering of Carbon Nanotube Bundles under Axial Strain and Strain-Induced Debundling. *Phys. Rev. B: Condens. Matter Mater. Phys.* **2007**, *75*, 155421−155424.
(37) Liu, Z. F.; Zhang, J.; Gao, B. Raman Spectroscopy of Strained Single-Walled Carbon Nanotubes. *Chem. Commun.* **2009**, *45*, 6902−6918.
(38) Thomsen, C.; Reich, S.; Jantoljak, H.; Loa, I.; Syassen, K.; Burghard, M.; Duesberg, G. S.; Roth, S. Raman Spectroscopy on Single- and Multi-Walled Nanotubes under High Pressure. *Appl. Phys. A: Mater. Sci. Process.* **1999**, *69*, 309−312.
(39) Park, J.; Yan, M. Covalent Functionalization of Graphene with Reactive Intermediates. *Acc. Chem. Res.* **2012**, *46*, 181−189.

DOI: 10.1021/acsami.5b07064
ACS Appl. Mater. Interfaces 2015, 7, 21602−21609